

Prevalence of two-dimensional photonic topology

Ali Ghorashi,^{1,*} Sachin Vaidya,^{1,2} Mikael Rechtsman,² Wladimir Benalcazar,³ Marin Soljačić,¹ and Thomas Christensen^{1,4,†}

¹*Department of Physics, Massachusetts Institute of Technology, Cambridge, MA 02139, USA*

²*Department of Physics, The Pennsylvania State University, University Park, PA 16801*

³*Department of Physics, Emory University, Atlanta, GA 30322, USA*

⁴*Department of Photonics and Electrical Engineering, Technical University of Denmark, Lyngby 2800, Denmark*

The topological characteristics of photonic crystals have been the subject of intense research in recent years. Despite this, the basic question of whether photonic band topology is rare or abundant—i.e., its relative prevalence—remains unaddressed. Here, we determine the prevalence of stable, fragile, and higher-order photonic topology in the 11 two-dimensional crystallographic symmetry settings that admit diagnosis of one or more of these phenomena by symmetry analysis. Our determination is performed on the basis of a data set of 550 000 randomly sampled, two-tone photonic crystals, spanning 11 symmetry settings and 5 dielectric contrasts, and examined in both transverse electric (TE) and magnetic (TM) polarizations. We report the abundance of nontrivial photonic topology in the presence of time-reversal symmetry and find that stable, fragile, and higher-order topology are generally abundant. Below the first band gap, which is of primary experimental interest, we find that stable topology is more prevalent in the TE polarization than the TM; is only weakly, but monotonically, dependent on dielectric contrast; and that fragile topology is near-absent. In the absence of time-reversal symmetry, nontrivial Chern phases are also abundant in photonic crystals with 2-, 4-, and 6-fold rotational symmetries but comparatively rare in settings with only 3-fold symmetry. Our results elucidate the interplay of symmetry, dielectric contrast, electromagnetic polarization, and time-reversal breaking in engendering topological photonic phases and may inform general design principles for their experimental realization.

Topological properties of photonic crystals (PhCs) [1, 2] have attracted substantial interest since the prediction of topological insulators in electronic systems [3, 4]. In particular, recent research has run the gamut of time-reversal (T) invariant and broken topology, ranging across topological degeneracies [5], Chern phases [6–8], higher-order topology [9, 10], and beyond. Here, we investigate the prevalence of stable, fragile, and higher-order photonic topology in all two-dimensional (2D) symmetry settings that admit their symmetry-based identification. In this pursuit, we create a data base of topological 2D PhCs, analogous to recent data bases of electronic and phononic materials [11–16].

Our work is motivated by the following simple questions: How prevalent is topology in 2D PhCs in a statistical sense? How is this prevalence affected by dielectric contrast, symmetries, and mode polarization? Are certain regions of the photonic band structure more likely to be topological than others? Answering these questions is of fundamental importance for the understanding, design, and experimental realization of photonic topological phenomena, because an understanding of the parameter space of topology can inform general design principles—e.g., the symmetries, geometric features, and range of dielectric contrasts most advantageous to engendering topological phases. To address these questions, we adopt the recent frameworks of topological quantum chemistry (TQC) [17, 18] and symmetry indicators [19–21], which have recently seen application and adaption also to the photonic context [22–28]. Their highly efficient and broadly-applicable qualities naturally lend them to high-throughput calculations, enabling us to answer the above questions by directly and comprehensively sampling the design space of 2D PhCs.

Methods. We briefly summarize the salient ideas of the symmetry-based approach, which diagnoses topology from the ability to decompose a set of bands into linear combinations of

so-called elementary band representations (EBRs) [29]. These EBRs span the space of symmetry-respecting atomic limits (symmetric, exponentially localized Wannier orbitals). Conceptually, if a set of bands—a multiplet—cannot be expressed as a “stack” of EBRs, there is a topological obstruction to smoothly deforming the multiplet to an atomic limit. More technically, given a trivial multiplet \mathfrak{n} in a PhC with plane group symmetry G , \mathbf{k} -wise gapped from all other bands, there exists a symmetry- and gap-preserving equivalence relation between \mathfrak{n} and a decomposition in the EBRs of G [18–20]:

$$\mathfrak{n} \sim \bigoplus_{\mathbf{q}\alpha} m_{\mathbf{q}}^{\alpha}(\mathbf{q}|D_{\mathbf{q}}^{\alpha}). \quad (1)$$

Here, $(\mathbf{q}|D_{\mathbf{q}}^{\alpha})$ denotes an EBR induced from a maximal Wyck-off position \mathbf{q} in G , transforming like the α th irreducible representation (irrep) $D_{\mathbf{q}}^{\alpha}$ of the associated site-symmetry group $G_{\mathbf{q}} \equiv \{g \in G \mid g\mathbf{q} = \mathbf{q}\}$, and $m_{\mathbf{q}}^{\alpha} \in \{0, 1, 2, \dots\}$ is the decomposition’s EBR multiplicity.

The key simplification of symmetry-based frameworks [18–20] is to relax the strict functional decomposition of Eq. (1) to a decomposition of band symmetries. In detail, we decompose the so-called symmetry vector \mathbf{n} of \mathfrak{n} —enumerating the symmetry content of \mathfrak{n} through the multiplicities $n_{\mathbf{k}}^{\alpha}$ of little group irreps $D_{\mathbf{k}}^{\alpha}$ across all high-symmetry \mathbf{k} -points—into the symmetry vectors of $(\mathbf{q}|D_{\mathbf{q}}^{\alpha})$ —which, to ease notation, we shall denote by the same symbol—according to:

$$\mathbf{n} = \sum_{\mathbf{q}\alpha} c_{\mathbf{q}}^{\alpha}(\mathbf{q}|D_{\mathbf{q}}^{\alpha}). \quad (2)$$

The symmetry-inferable topological diagnosis is made on the basis of the decomposition coefficients $c_{\mathbf{q}}^{\alpha}$ [20, 30, 31] (Fig. 1ab): if all $c_{\mathbf{q}}^{\alpha}$ can be chosen as non-negative integers, \mathfrak{n} is compatible with the symmetries of an atomic limit, i.e., nominally topologically trivial [32]. If the decomposition must

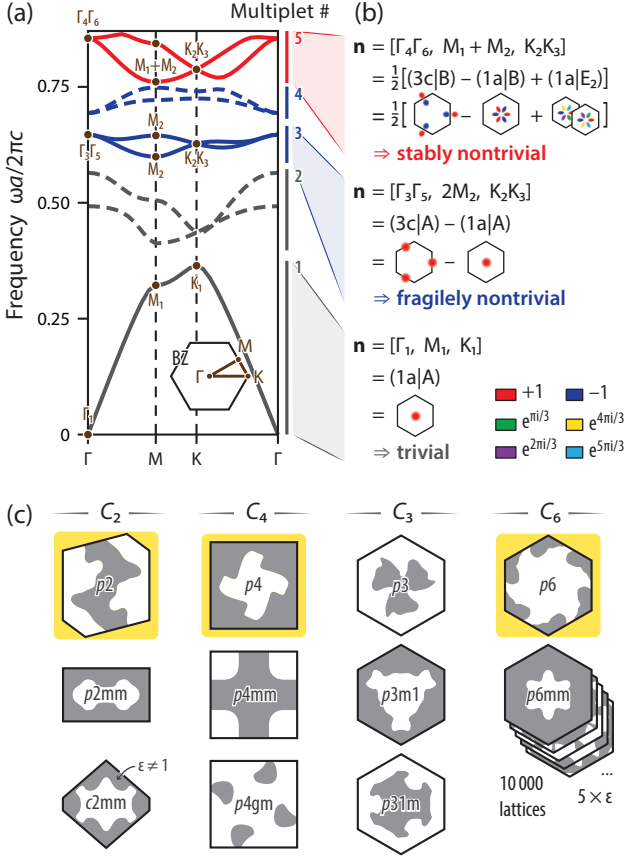


Figure 1. Methodology, workflow, and data set (a) Band structure of a $p6$ -symmetric PhC, hosting 5 separable bands, i.e., multiplets (TE polarization, unit cell from (c)). (b) For each multiplet, we decompose the symmetry vectors, \mathbf{n} , in EBRs to obtain a symmetry-based diagnosis of band topology from the decomposition’s coefficients. (c) Examples of PhC unit cells in our data set, spanning 11 plane groups, each labelled in Hermann–Mauguin notation [37] and grouped by their rotational symmetry (C_n). Groups that admit stable, T -invariant topology are highlighted in yellow.

include EBRs that are not centered at the unit cell origin, \mathbf{n} is also said to be an obstructed atomic limit, which may host nonzero bulk polarization or corner charges with corresponding filling anomalies [25]. Conversely, if a decomposition exists with integer c_q^α but requiring at least one negative coefficient, \mathbf{n} is topologically fragile [33]: by addition of appropriate atomic limits (namely, the EBRs associated with negative c_q^α), the band topology can be trivialized. In contrast to this, if the decomposition requires non-integer, rational c_q^α , the topology of \mathbf{n} is stably nontrivial [17]—being trivializable only by other nontrivial bands. If no decomposition exists, \mathbf{n} describes a set of band symmetries that are inconsistent with compatibility relations [34], i.e., a set of bands that are not gapped along high-symmetry \mathbf{k} -lines. We implemented a software package, MPBUutils.jl [35], written in the Julia language, to facilitate this analysis, allowing automatic clustering and topological diagnosis of compatibility-respecting photonic bands [36].

PhC data set. Of the 17 plane groups that describe the symmetry settings of 2D PhCs, only 11 allow symmetry-based distinc-

tions between trivial and fragile or stable topology [20, 31], namely those with a proper subgroup of $C_{n \geq 2}$. For each of these 11 plane groups, we created 10 000 unique, randomly-generated PhC unit cells using a Fourier-based level-set technique [23, 38] (Fig. 1c and Supplemental Section S10). Summarizing, we consider a “two-tone” dielectric motif in each unit cell: in one region, we place vacuum and in the other a dielectric with permittivity ε , scanning parametrically across $\varepsilon \in \{8, 12, 16, 24, 32\}$, with a filling fraction randomly sampled from a uniform distribution between 0.2 and 0.8. For each PhC, we compute the requisite band symmetries at high-symmetry \mathbf{k} -points for the first 40 bands, using the MIT Photonic Bands solver [39] and the tooling developed in Ref. 23, for both transverse electric (TE) and magnetic (TM) polarizations, obtaining the corresponding symmetry vectors of each separable multiplet (Fig. 2ab). Finally, each multiplet’s symmetry-diagnosable band topology is determined via Eq. (2). Altogether, our data set encompasses 11 (symmetry) \times 10 000 (motif) \times 5 (contrast) \times 2 (polarization) = 1 100 000 distinct calculations. For a 64×64 discretization grid and 40 bands, a typical single-core calculation takes on the order of 20 s.

Stable and fragile topology. Figure 2 summarizes our results on the prevalence of stable and fragile topology in T -invariant 2D PhCs. We report the prevalence of band topology multiplet-by-multiplet as opposed to cumulatively (i.e., up to and including the n th multiplet), because cumulative fragile topology is near-absent, as we explain later (Supplemental Section S6 reports cumulative statistics).

We focus first on stable topology, which is symmetry-diagnosable in just three plane groups—namely, $p2$, $p4$, and $p6$ (i.e., with $C_{n=2,4,6}$ -symmetric unit cells) [20]—and associated with an odd number of Dirac points in each n -fold symmetric BZ-sector (equivalently, a π Berry phase for loops encircling such sectors) [40, 41]. Figure 2a summarizes our results for a fixed permittivity of $\varepsilon = 16$ for the dielectric region. Surprisingly, stable topology is widely prevalent. E.g., given a random PhC in $p2$, one should expect Dirac points with a likelihood of ~ 30 – 50 %, depending on multiplet and polarization. We emphasize that these Dirac points are qualitatively different from the more familiar doublet of Dirac points at the BZ boundary (K and K’ points) of C_6 -symmetric settings [42, 43]: here, instead, there are $n \bmod 2n$ Dirac points in the BZ interior (Fig. 2b). Polarization-wise, we find that stable topology is more prevalent in the TE than the TM polarization, especially evident in $p4$ and $p6$ where stable topology in the first TM multiplet is near-absent. Further, varying the permittivity of the dielectric region (Fig. 2c), we observe that the overall prevalence is only weakly dependent on dielectric contrast: physically, dielectric contrast mainly controls the size of band gaps—affecting band symmetries and topology only if multiple band closures separate the band structure from the empty-lattice limit. I.e., geometry is the main design variable for engendering stable PhC topology. The prevalence of frequency-isolatable Dirac points—i.e., Dirac points whose frequency do not intersect other bulk bands—is a small fraction of the overall prevalence of stable topology, however

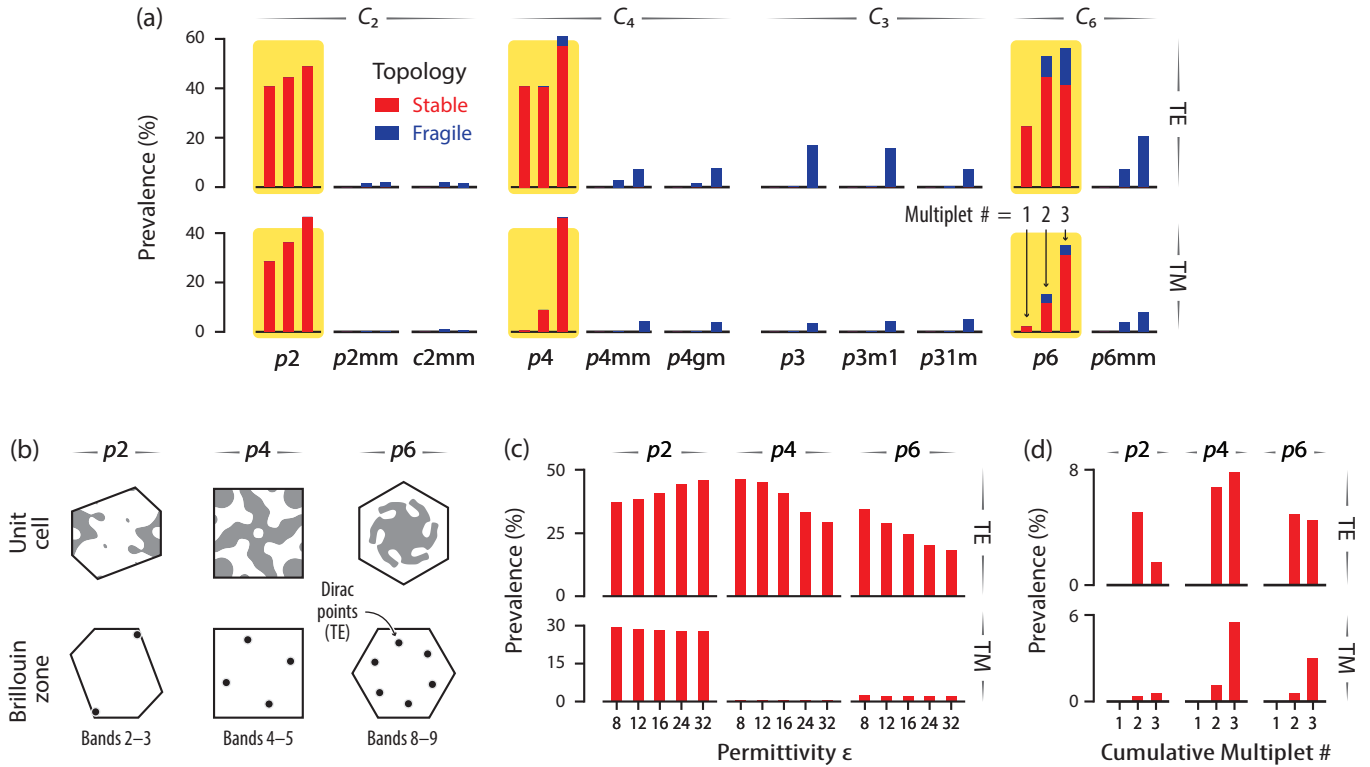


Figure 2. Prevalence of stable and fragile time-reversal invariant topology. (a) Prevalence of symmetry-identifiable stable and fragile topology across plane groups (permittivity $\epsilon = 16$; prevalence reported multiplet-by-multiplet). Plane groups that allow symmetry-based identification of stable topology are highlighted in yellow. (b) Examples of three PhCs with stable topology and associated Dirac points at generic \mathbf{k} -points (TE polarization). The selected examples have no intersecting trivial bulk “Fermi pockets”, i.e., the Dirac points are frequency-isolated. (c) Permittivity-dependence of stable topology in p_2 , p_4 , and p_6 for the first multiplet. (d) Fraction of cumulatively stable multiplets whose associated Dirac points are frequency-isolated. A near-complete absence is observed in the first multiplet.

(Fig. 2d and Supplemental Section S12): near-vanishing in the first multiplet and at most a few percent in higher multiplets.

Unlike stable topology, fragile topology is symmetry-diagnosable in all 11 plane groups (Fig. 2a). Although far less prevalent than its stable counterpart, several plane groups feature a substantial prevalence of fragile multiplets, especially among higher multiplets. We find fragile multiplets in settings with both C_2T symmetry (with relatively winding “straight” Wilson loops and a nontrivial Euler class [17]) and C_3 symmetry (with relatively winding “concentric” Wilson loops [44, 45]). However, we find a near-complete dearth of cumulatively fragile multiplets: across our entire data set, we identify just 43 PhCs with cumulatively fragile topology, all with equivalent EBR decompositions (Supplemental Section S7). Despite recent progress [46–50], the observable consequences of cumulatively fragile topology remains largely an open question, especially in PhCs [22, 51]. Here, analyzing each cumulatively fragile PhC separately, we find that the corresponding bands feature *pairs* of nodal points in each n -fold symmetric sector of the Brillouin zone (Supplemental Section S7).

Higher-order topology. Beyond the symmetry-indicated classifications of stable, fragile, and trivial (i.e., atomic limits) band topology [18–20] exists a finer gradation associated with higher-order topology and filling anomalies [52]. In particular,

a filling anomaly exists in any finite C_n -symmetric tiling of a PhC unit cell with nonzero bulk polarization (\mathbf{P}) or corner charge (Q) associated with fractional mode densities at the tiling’s edges or corners, respectively. In turn, \mathbf{P} and Q can be evaluated from band symmetry [52]—or, equivalently, from the EBR decompositions of Eq. (2) (Supplemental Section S3).

We give values of \mathbf{P} and Q in dimensionless units below, dispensing with the customary-charge prefactor relevant to electronic systems: i.e., Q is defined modulo 1 and \mathbf{P} modulo direct lattice vectors.

We restrict our attention to multiplets with nominally trivial cumulative topology, i.e., non-negative EBR decomposition coefficients, corresponding to bands that are symmetry-compatible with a gapped atomic limit. For these multiplets, we classify a given PhC unit cell as higher-order nontrivial if there exists a unit-cell centering choice with vanishing bulk polarization ($\mathbf{P} = \mathbf{0}$) and nonzero corner charge ($Q \neq 0$). This definition is motivated by the following considerations: (1) Unlike assignment of stable and fragile band topology, \mathbf{P} and Q are generally dependent on the choice of unit-cell centering (Supplemental Section S1) [53]. (2) By requiring $\mathbf{P} = \mathbf{0}$ we ensure that a $Q \neq 0$ filling anomaly is strictly isolated to corner states, and not coexisting with a corresponding edge anomaly [25, 52, 54–56]; additionally, if $\mathbf{P} \neq \mathbf{0}$, the definition

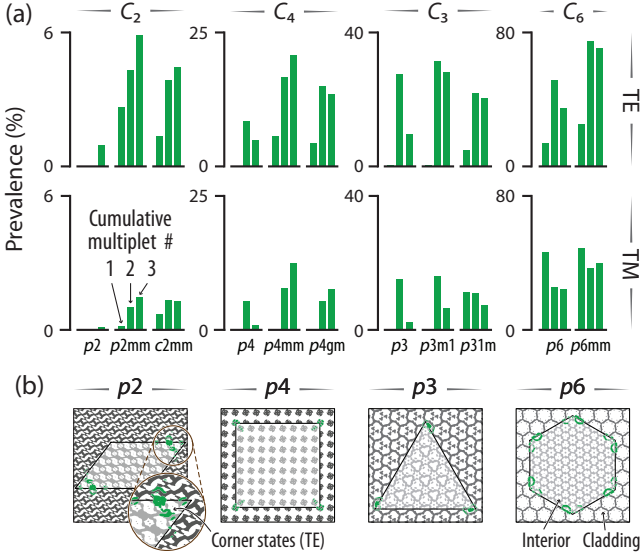


Figure 3. Prevalence of corner charges. (a) Prevalence of cumulative higher-order topology, as defined in the main text. (b) Supercell simulations of selected PhC samples with corner charges, cladded by suitable atomic-limit PhCs (Supplemental Section S13), in $p2$, $p4$, $p3$, and $p6$. Contours of energy density shown in green.

of Q is dependent on the tiling’s boundary configuration in C_3 -symmetric settings (Supplemental Section S8). In practice, for a PhC unit cell with a C_n subgroup symmetry, we evaluate \mathbf{P} and Q for each centering choice that preserves a C_n axis at the unit-cell center, registering the sample’s multiplet as higher-order nontrivial if any such centering allows $\mathbf{P} = \mathbf{0}$ and $Q \neq 0$, jointly with an absence of stable or fragile topology.

Figure 3 reports the prevalence of higher-order topology consistent with this definition, along with supercell calculations of selected samples showcasing the associated corner filling anomaly. Broadly, prevalence is highest in plane groups with a C_6 subgroup, lowest in those with a C_2 subgroup, and intermediate those with a C_4 or C_3 subgroup. More specifically, we highlight two interesting features in specific plane groups: First, a complete absence of nontrivial higher-order topology is observed below the third multiplet in $p2$: this is because a $\{\mathbf{P} = \mathbf{0}, Q \neq 0\}$ multiplet requires 3 bands in C_2 - and C_4 -symmetric settings (Supplemental Section S4) while all $p2$ -multiplets are singly degenerate (unlike $p4$, accounting for the nonzero prevalence in its lower multiplets). Second, in plane groups $p31m$, $p6$, and $p6mm$, there always exists a centering choice that ensures $\mathbf{P} = \mathbf{0}$ (Supplemental Section S2). Considering this, it is natural to expect a higher prevalence of higher-order topology in these settings. However, $p31m$ mostly defies this expectation, suggesting that the prevalence of higher-order topology in $p6$ and $p6mm$ are predominately attributable to their higher rotational symmetry.

Time-reversal breaking and Chern topology. Thus far, we have focused entirely on T -invariant PhCs, which necessarily have trivial Chern topology. To assess the prevalence of nontrivial Chern phases under T -breaking, and focusing on the TE polarization [57], we incorporate a gyroelectric ef-

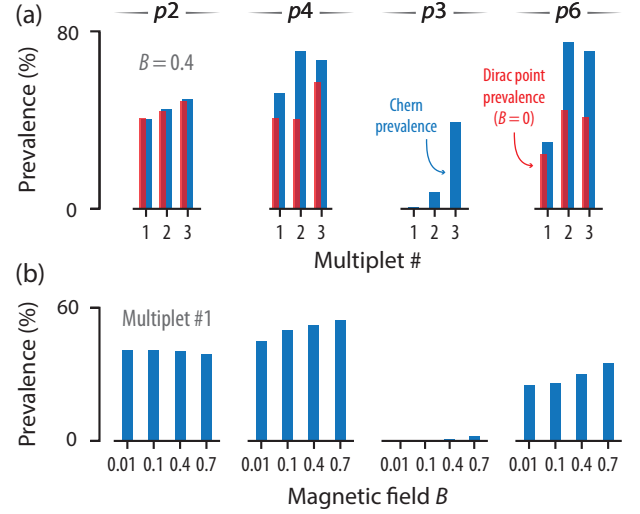


Figure 4. Prevalence of Chern topology under time-reversal breaking. (a) Prevalence of nontrivial Chern topology in the lowest three multiplets an effective magnetic field $B = 0.4$ for TE polarization in plane groups $p2$, $p3$, $p4$ and $p6$. (b) Prevalence of nontrivial Chern topology in the first multiplet as a function of magnetic field. Prevalence is reported multiplet-by-multiplet.

fect due to a \hat{z} -oriented external magnetic field. This lifts the scalar permittivity ε to an anisotropic, nonreciprocal tensor ε with off-diagonal and diagonal elements $\varepsilon_{xy} = -\varepsilon_{yx} = i\varepsilon B$ and $\varepsilon_{xx} = \varepsilon_{yy} = \varepsilon(1 + B^2)^{1/2}$, respectively, where B represents the effective magnetic field amplitude [5].

Fixing $\varepsilon = 16$ and restricting our attention to the C_n -symmetric plane groups— $p2$, $p4$, $p3$, and $p6$ —that admit a symmetry-based identification of the Chern number modulo n [40], we report the prevalence of nonzero Chern numbers in Fig. 4. For the first multiplet, the results can be understood (and approximately lower-bounded for small B), from the corresponding prevalence of Dirac points under T symmetry (Fig. 4a, red bars). Specifically, in 2D, the sources of Chern topology are Dirac [6] or quadratic degeneracies [58]. For example, in $p2$, the only such sources are Dirac points in the BZ interior: as a result, the prevalence of symmetry-identifiable stable T -invariant and T -broken nontrivial topology agrees exactly at small B . Conversely, $p4$ and $p6$ also allow T -protected Dirac and quadratic degeneracies at high-symmetry \mathbf{k} -points, contributing to a higher prevalence of Chern-nontrivial phases than their T -invariant counterparts. Unlike these plane groups, $p3$ does not support robust Dirac points due to its lack of 2-fold rotation symmetry. Instead, it admits a solitary quadratic degeneracy associated with the $\Gamma_2\Gamma_3$ irrep, whose T -breaking can realize nontrivial Chern topology. The first multiplet of $p3$, however, is singly degenerate and so never includes this irrep, thus explaining the complete absence of nonzero Chern numbers in the first multiplet.

For larger magnetic fields (Fig. 4b), this simple understanding of breaking T -protected degeneracies is modified by the potential for driving multiple band inversions as B is increased. In the aggregate, however, i.e., as an impact on overall prevalence, the influence of T -breaking strength appears modest

since such inversions tend to produce changes of the band topology that average out over distinct PhC samples.

Discussion. By comprehensively sampling the space of symmetric 2D PhCs, we have investigated the relative abundance of stable, fragile, and higher-order photonic topology. Our work elucidates the extent to which various experimental parameters, such as polarization, dielectric contrast, T -breaking strength, symmetry, and geometry relate to the prevalence of topological band phenomena. Overall, we find that this prevalence is affected mainly by polarization, symmetry, and geometry. Contrary to the prevalent association of photonic topology with exotic or rare phenomena—but consistently with recent results from the electronic and phononic domains [11–16]—we conclude that photonic topology is very prevalent, even common. Certain photonic topological features, most notably cumulatively fragile topology, remain rare, however.

Our work motivates future investigations along several lines [59]. For instance, can a partial theoretical understanding be established for the observed statistics, e.g., via the empty-lattice approximation? What is the physical reason for the near-absence of cumulative fragile topology? And, within a particular symmetry setting, which geometrical motifs are most associated with topological band features? Our data set [60] may also serve as the foundations for machine-learning-centric investigations into topological physics [61] and photonics [38, 62, 63]. Finally, the prevalence observed in our work highlights that the main design challenge of photonic topology is one of finding desired band topology *jointly* with desired spectral properties, e.g., large topological gaps or well-isolated degeneracies, motivating further research in topological inverse design [24, 64].

The data and code used to obtain and analyze the results presented here are made available online [60].

A.G. acknowledges the support of the National Science Foundation Graduate Research Fellowship (GRFP). T.C. acknowledges the support of a research grant (project no. 42106) from Villum Fonden. This research is based upon work supported in part by the Air Force Office of Scientific Research under Grant No. FA9550-20-1-0115 and FA9550-21-1-0299, the U.S. Office of Naval Research (ONR) Multidisciplinary University Research Initiative (MURI) Grant No. N00014-20-1-2325 on Robust Photonic Materials with High-Order Topological Protection, and the U.S. Army Research Office through the Institute for Soldier Nanotechnologies at MIT under Collaborative Agreement No. W911NF-18-2-0048. The MIT SuperCloud and Lincoln Laboratory Supercomputing Center provided computing resources that contributed to the results reported in this work.

* aligho@mit.edu

† thomas@dtu.dk

[1] L. Lu, J. D. Joannopoulos, and M. Soljačić, Topological photonics, *Nat. Photon.* **8**, 821 (2014).

- [2] T. Ozawa, H. M. Price, A. Amo, N. Goldman, M. Hafezi, L. Lu, M. C. Rechtsman, D. Schuster, J. Simon, O. Zilberberg, and I. Carusotto, Topological photonics, *Rev. Mod. Phys.* **91**, 015006 (2019).
- [3] L. Fu, C. L. Kane, and E. J. Mele, Topological insulators in three dimensions, *Phys. Rev. Lett.* **98**, 106803 (2007).
- [4] C. L. Kane and E. J. Mele, Quantum spin Hall effect in graphene, *Phys. Rev. Lett.* **95**, 226801 (2005).
- [5] L. Lu, L. Fu, J. D. Joannopoulos, and M. Soljačić, Weyl points and line nodes in gyroid photonic crystals, *Nature Photonics* **7**, 294 (2013).
- [6] F. D. M. Haldane and S. Raghu, Possible realization of directional optical waveguides in photonic crystals with broken time-reversal symmetry, *Phys. Rev. Lett.* **100**, 013904 (2008).
- [7] Z. Wang, Y. Chong, J. D. Joannopoulos, and M. Soljačić, Observation of unidirectional backscattering-immune topological electromagnetic states, *Nature* **461**, 772 (2009).
- [8] S. A. Skirlo, L. Lu, Y. Igarashi, Q. Yan, J. Joannopoulos, and M. Soljačić, Experimental observation of large Chern numbers in photonic crystals, *Phys. Rev. Lett.* **115**, 253901 (2015).
- [9] L. He, Z. Addison, E. J. Mele, and B. Zhen, Quadrupole topological photonic crystals, *Nature Commun.* **11**, 3119 (2020).
- [10] B.-Y. Xie, H.-F. Wang, H.-X. Wang, X.-Y. Zhu, J.-H. Jiang, M.-H. Lu, and Y.-F. Chen, Second-order photonic topological insulator with corner states, *Phys. Rev. B* **98**, 205147 (2018).
- [11] T. Zhang, Y. Jiang, Z. Song, H. Huang, Y. He, Z. Fang, H. Weng, and C. Fang, Catalogue of topological electronic materials, *Nature* **566**, 475 (2019).
- [12] F. Tang, H.C. Po, A. Vishwanath, and X. Wan, Comprehensive search for topological materials using symmetry indicators, *Nature* **566**, 486 (2019).
- [13] M. Vergniory, L. Elcoro, C. Felser, N. Regnault, B.A. Bernevig, and Z. Wang, A complete catalogue of high-quality topological materials, *Nature* **566**, 480 (2019).
- [14] M. G. Vergniory, B. J. Wieder, L. Elcoro, S. S. P. Parkin, C. Felser, B. A. Bernevig, and N. Regnault, All topological bands of all nonmagnetic stoichiometric materials, *Science* **376**, eabg9094 (2022).
- [15] J. Sødequist, U. Petralanda, and T. Olsen, Abundance of second order topology in C_3 symmetric two-dimensional insulators, *2D Materials* **10**, 015009 (2022).
- [16] Y. Xu, M. G. Vergniory, D.-S. Ma, J. L. Mañes, Z.-D. Song, B. A. Bernevig, N. Regnault, and L. Elcoro, Catalogue of topological phonon materials, *arXiv:2211.11776* (2022).
- [17] J. Cano and B. Bradlyn, Band representations and topological quantum chemistry, *Annu. Rev. Condens. Matter Phys.* **12**, 225 (2021).
- [18] B. Bradlyn, L. Elcoro, J. Cano, M. G. Vergniory, Z. Wang, C. Felser, M. I. Aroyo, and B. A. Bernevig, Topological quantum chemistry, *Nature* **547**, 298 (2017).
- [19] J. Kruthoff, J. de Boer, J. van Wezel, C. L. Kane, and R.-J. Slager, Topological classification of crystalline insulators through band structure combinatorics, *Phys. Rev. X* **7**, 041069 (2017).
- [20] H. C. Po, A. Vishwanath, and H. Watanabe, Symmetry-based indicators of band topology in the 230 space groups, *Nature Commun.* **8**, 50 (2017).
- [21] H. C. Po, Symmetry indicators of band topology, *Journal of Physics: Condensed Matter* **32**, 263001 (2020).
- [22] M. B. De Paz, M. G. Vergniory, D. Bercioux, A. García-Etxarri, and B. Bradlyn, Engineering fragile topology in photonic crystals: Topological quantum chemistry of light, *Phys. Rev. Res.* **1**, 032005 (2019).
- [23] T. Christensen, H. C. Po, J. D. Joannopoulos, and M. Soljačić, Location and topology of the fundamental gap in photonic crystals, *Phys. Rev. X* **12**, 021066 (2022).

- [24] S. Kim, T. Christensen, S. G. Johnson, and M. Soljačić, Automated discovery and optimization of 3D topological photonic crystals, *ACS Photonics* **10**, 861 (2023).
- [25] S. Vaidya, A. Ghorashi, T. Christensen, M. C. Rechtsman, and W. A. Benalcazar, Topological phases of photonic crystals under crystalline symmetries, [arXiv:2303.10261](https://arxiv.org/abs/2303.10261) (2023).
- [26] S. Vaidya, M. C. Rechtsman, and W. A. Benalcazar, Response to polarization and weak topology in Chern insulators, [arXiv:2304.13118](https://arxiv.org/abs/2304.13118) (2023).
- [27] A. Morales-Pérez, C. Devescovi, Y. Hwang, M. García-Díez, B. Bradlyn, J. L. Mañes, M. G. Vergniory, and A. García-Etxarri, Transversality-enforced tight-binding model for 3D photonic crystals aided by topological quantum chemistry, [arXiv:2305.18257](https://arxiv.org/abs/2305.18257) (2023).
- [28] C. Devescovi, A. Morales-Pérez, Y. Hwang, M. García-Díez, I. Robredo, J. L. Mañes, B. Bradlyn, A. García-Etxarri, and M. G. Vergniory, Axion topology in photonic crystal domain walls, [arXiv:2305.19805](https://arxiv.org/abs/2305.19805) (2023).
- [29] J. Zak, Band representations of space groups, *Phys. Rev. B* **26**, 3010 (1982).
- [30] L. Elcoro, Z. Song, and B. A. Bernevig, Application of induction procedure and Smith decomposition in calculation and topological classification of electronic band structures in the 230 space groups, *Phys. Rev. B* **102**, 035110 (2020).
- [31] Z.-D. Song, L. Elcoro, Y.-F. Xu, N. Regnault, and B. A. Bernevig, Fragile phases as affine monoids: classification and material examples, *Phys. Rev. X* **10**, 031001 (2020).
- [32] While a non-negative integer decomposition in Eq. (1) is a strict definition of topological triviality, the same is not true for the decompositions in Eq. (2). Rather, such a decomposition only implies compatibility with the band symmetries of a trivial atomic limit, not necessarily trivial band topology [20]: we call this “nominally trivial”. E.g., in T -broken PhCs with C_n symmetry, a symmetry-based diagnosis of triviality implies only that the Chern number vanishes modulo n . However, an inability to find non-negative integer decompositions in Eq. (2), is a strict implication of nontrivial band topology, either fragile or stable. Because of this, our symmetry-based assessments of topological prevalence in fact represent lower bounds.
- [33] H. C. Po, H. Watanabe, and A. Vishwanath, Fragile topology and Wannier obstructions, *Phys. Rev. Lett.* **121**, 126402 (2018).
- [34] L. P. Bouckaert, R. Smoluchowski, and E. Wigner, Theory of Brillouin zones and symmetry properties of wave functions in crystals, *Phys. Rev.* **50**, 58 (1936).
- [35] MPBUtils.jl (v0.1.11), <https://github.com/thchr/MPBUtils.jl>, accessed 25 July, 2023.
- [36] The 2D PhC problem is spared the complications of the Γ -point band-symmetry assignment issues of 3D PhCs [23]. Instead, the polarization of TE and TM modes imply a natural rule [22]: in the zero-frequency at Γ , the TM (TE) band transform as a \hat{z} -oriented vector (pseudovector).
- [37] M. I. Aroyo, ed., *International Tables for Crystallography Volume A: Space-group Symmetry*, 6th ed. (Wiley, 2016).
- [38] T. Christensen, C. Loh, S. Picek, D. Jakobović, L. Jing, S. Fisher, V. Ceperic, J. D. Joannopoulos, and M. Soljačić, Predictive and generative machine learning models for photonic crystals, *Nanophotonics* **9**, 4183 (2020).
- [39] S. G. Johnson and J. D. Joannopoulos, Block-iterative frequency-domain methods for Maxwell’s equations in a planewave basis, *Opt. Express* **8**, 173 (2001).
- [40] C. Fang, M. J. Gilbert, and B. A. Bernevig, Bulk topological invariants in noninteracting point group symmetric insulators, *Phys. Rev. B* **86**, 115112 (2012).
- [41] Z. Song, T. Zhang, and C. Fang, Diagnosis for nonmagnetic topological semimetals in the absence of spin-orbital coupling, *Phys. Rev. X* **8**, 031069 (2018).
- [42] G. W. Semenoff, Condensed-matter simulation of a three-dimensional anomaly, *Phys. Rev. Lett.* **53**, 2449 (1984).
- [43] T. Ochiai and M. Onoda, Photonic analog of graphene model and its extension: Dirac cone, symmetry, and edge states, *Phys. Rev. B* **80**, 155103 (2009).
- [44] B. Bradlyn, Z. Wang, J. Cano, and B. A. Bernevig, Disconnected elementary band representations, fragile topology, and Wilson loops as topological indices: An example on the triangular lattice, *Phys. Rev. B* **99**, 045140 (2019).
- [45] J. G. B. Henke, *Topology in crystals and symmetry-breaking from interactions*, Ph.D. thesis, Institute for Theoretical Physics, University of Amsterdam (2022).
- [46] Y. Hwang, J. Ahn, and B.-J. Yang, Fragile topology protected by inversion symmetry: Diagnosis, bulk-boundary correspondence, and Wilson loop, *Phys. Rev. B* **100**, 205126 (2019).
- [47] Z.-D. Song, L. Elcoro, and B. A. Bernevig, Twisted bulk-boundary correspondence of fragile topology, *Science* **367**, 794 (2020).
- [48] V. Peri, Z.-D. Song, M. Serra-Garcia, P. Engeler, R. Queiroz, X. Huang, W. Deng, Z. Liu, B. A. Bernevig, and S. D. Huber, Experimental characterization of fragile topology in an acoustic metamaterial, *Science* **367**, 797 (2020).
- [49] F. N. Ünal, A. Bouhon, and R.-J. Slager, Topological Euler class as a dynamical observable in optical lattices, *Phys. Rev. Lett.* **125**, 053601 (2020).
- [50] G. F. Lange, A. Bouhon, and R.-J. Slager, Subdimensional topologies, indicators, and higher order boundary effects, *Phys. Rev. B* **103**, 195145 (2021).
- [51] A. Alexandradinata, J. Höller, C. Wang, H. Cheng, and L. Lu, Crystallographic splitting theorem for band representations and fragile topological photonic crystals, *Phys. Rev. B* **102**, 115117 (2020).
- [52] W. A. Benalcazar, T. Li, and T. L. Hughes, Quantization of fractional corner charge in C_n -symmetric higher-order topological crystalline insulators, *Phys. Rev. B* **99**, 245151 (2019).
- [53] R. Takahashi, T. Zhang, and S. Murakami, General corner charge formula in two-dimensional C_n -symmetric higher-order topological insulators, *Phys. Rev. B* **103**, 205123 (2021).
- [54] F. Schindler, M. Brzezińska, W. A. Benalcazar, M. Iraola, A. Bouhon, S. S. Tsirkin, M. G. Vergniory, and T. Neupert, Fractional corner charges in spin-orbit coupled crystals, *Phys. Rev. Res.* **1**, 033074 (2019).
- [55] W. A. Benalcazar, B. A. Bernevig, and T. L. Hughes, Quantized electric multipole insulators, *Science* **357**, 61 (2017).
- [56] W. A. Benalcazar, B. A. Bernevig, and T. L. Hughes, Electric multipole moments, topological multipole moment pumping, and chiral hinge states in crystalline insulators, *Phys. Rev. B* **96**, 245115 (2017).
- [57] The TM modes are unaffected by the considered gyroelectric effect, since their \mathbf{E} -fields are \hat{z} -oriented. An analogous gyromagnetic effect with nonreciprocal permeability, i.e., with $\mu_{xy} = -\mu_{yx}$, breaks T for the TM polarized bands [7, 65].
- [58] Y. D. Chong, X.-G. Wen, and M. Soljačić, Effective theory of quadratic degeneracies, *Phys. Rev. B* **77**, 235125 (2008).
- [59] As we were finalizing this manuscript, we became aware of related work under preparation [66].
- [60] <https://github.com/AlighorashiCMT/Topological-Prevalence>, accessed 26 July, 2023.
- [61] A. Ma, Y. Zhang, T. Christensen, H. C. Po, L. Jing, L. Fu, and M. Soljačić, Topogivity: A machine-learned chemical rule for discovering topological materials, *Nano Lett.* **23**, 772 (2023).
- [62] C. Loh, T. Christensen, R. Dangovski, S. Kim, and M. Soljačić, Surrogate- and invariance-boosted contrastive learning for data-scarce applications in science, *Nat. Commun.* **13**, 4223 (2022).

- [63] O. Khatib, S. Ren, J. Malof, and W. J. Padilla, Deep learning the electromagnetic properties of metamaterials—a comprehensive review, *Adv. Funct. Mater.* **31**, 2101748 (2021).
- [64] R. E. Christiansen, F. Wang, O. Sigmund, and S. Stobbe, Designing photonic topological insulators with quantum-spin-Hall edge states using topology optimization, *Nanophotonics* **8**, 1363 (2019).
- [65] Z. Wang, Y. D. Chong, J. D. Joannopoulos, and M. Soljačić, Reflection-free one-way edge modes in a gyromagnetic photonic crystal, *Phys. Rev. Lett.* **100**, 013905 (2008).
- [66] S. D. Huber, High-throughput generation of topological metamaterials, in *13th International Conference on Metamaterials, Photonic Crystals and Plasmonics* (2023) p. 781.